npj computational materials

www.nature.com/npjcompumats

ARTICLE OPEN

Check for updates

Machine learning assisted design of shape-programmable 3D kirigami metamaterials

Nicolas A. Alderete[1,3], Nibir Pathak[1,3] and Horacio D. Espinosa[1,2]✉

Kirigami-engineering has become an avenue for realizing multifunctional metamaterials that tap into the instability landscape of planar surfaces embedded with cuts. Recently, it has been shown that two-dimensional Kirigami motifs can unfurl a rich space of out-of-plane deformations, which are programmable and controllable across spatial scales. Notwithstanding Kirigami's versatility, arriving at a cut layout that yields the desired functionality remains a challenge. Here, we introduce a comprehensive machine learning framework to shed light on the Kirigami design space and to rationally guide the design and control of Kirigami-based materials from the meta-atom to the metamaterial level. We employ a combination of clustering, tandem neural networks, and symbolic regression analyses to obtain Kirigami that fulfills specific design constraints and inform on their control and deployment. Our systematic approach is experimentally demonstrated by examining a variety of applications at different hierarchical levels, effectively providing a tool for the discovery of shape-shifting Kirigami metamaterials.

npj Computational Materials (2022)8:191 ; https://doi.org/10.1038/s41524-022-00873-w

INTRODUCTION

The recent rediscovery of Japanese Kirigami by the engineering community has ushered in a new era in the field of flexible and reconfigurable surfaces, enabling diverse multiscale applications in soft robotics[1,2], stretchable electronics[3,4], optics[5], and textiles[6]. Underlying the potential of Kirigami-engineering lies a simple concept: the purposeful introduction of cuts in thin sheets subject to tension produces nonlinear responses (i.e., bifurcations) that preclude failure and break the sheet's bidimensionality to yield three-dimensional surfaces. However, the simplicity of Kirigami is only apparent, with recent numerical and experimental investigations showing that slight variations within a common geometric motif can result in variegated symmetric and anti-symmetric three-dimensional shapes[7], displaying three-dimensional tilts and twists, that can be controlled via quasi-static stretching[8]. While this rich landscape of deformed configurations makes Kirigami-based designs a fertile ground for shape-morphable applications, systematic methods to arrive at Kirigami motifs that fullfil a design requirement (i.e., inverse design problem) have been scarce, with trial-and-error (based on time-consuming experimental and computational iterations) remaining the prevalent approach. The inverse problem in the realm of Kirigami metamaterials has primarily been tackled using optimization methods[9–11], which have been shown to be successful but can be time-consuming, especially in highly nonlinear problems involving buckling, as for each new optimization target, the entire design space would have to be probed, which ultimately results in expensive computational iterations. Amid this paucity of approaches, data-driven methods pose an intriguing alternative for the exploration of vast design spaces in nonlinear mechanical metamaterials[12,13] and, particularly, for the solution to the complex Kirigami design problem. In this regard, the majority of efforts leveraging machine learning techniques have focused on the mechanical properties of Kirigami systems (e.g., yield strain/stress[14], ultimate stress/strain[15]), leaving the topological reconfigurability aspect and experimental validation unaddressed. Seeking to address this gap, which leaves Kirigami's most salient advantage over competing metamaterials untapped, we herein leverage an integral data-driven approach that aims to solve the Kirigami inverse-design problem at the meta-atom level, with implications and applications at the metamaterial level. More generally, in the area of mechanics and materials, the majority of data-driven approaches dealing with inverse design have mainly centered on individual attributes (e.g., design for energy absorption[16], spectral properties[17], toughness[18], etc.). In such studies, the sole focus was on the creation of a mapping from target properties to material design parameters, which are usually agnostic to the path between undeployed and deployed states[11]. In contrast, here we present and experimentally demonstrate a complete, systematic workflow for rational design, comprised of four concatenated modules: (1) exploration of the design space, (2) inverse design, (3) investigation of the conditions for deploying arrived-at designs and their tunability, and (4) utility to attain configurations outside the initial design space.

To illustrate the capabilities and potential of the proposed framework, we here focus on the same programmable and controllable Kirigami motif, previously investigated by ref. [7] and ref. [8], consisting of two inner panels delimited by a pair of internal line cuts and a pair of U-shaped cuts (Fig. 1). Though simple at first glance, prior investigations into this pattern have revealed a cornucopia of out-of-plane deformations exhibiting symmetry and symmetry-breaking behavior elicited by coincident and sequential bifurcations of the panels. The undeformed meta-atom geometry (Fig. 1 a, b) is completely defined by the sheet's length (L), width (W) and thickness (t), the length of the hinges (a_{1-4}), the height and width of the line and U-shaped cuts (h, w, c), and their distances to the exterior boundaries (d). In addition to the geometry, the mechanical response of the Kirigami is dictated by its elastic properties (Modulus E and Poisson's ratio, υ) and the degree of uniaxial stretch (σ).

Using the aforementioned Kirigami template as a meta-atom, the geometric design space is sampled employing a space-filling, quasi-random Sobol sequence. Employing the Kirigami geometries

[1]Theoretical and Applied Mechanics, Northwestern University, Evanston, IL 60208, USA. [2]Department of Mechanical Engineering, Northwestern University, Evanston, IL 60208, USA. [3]These authors contributed equally: Nicolas A. Alderete, Nibir Pathak. ✉email: espinosa@northwestern.edu

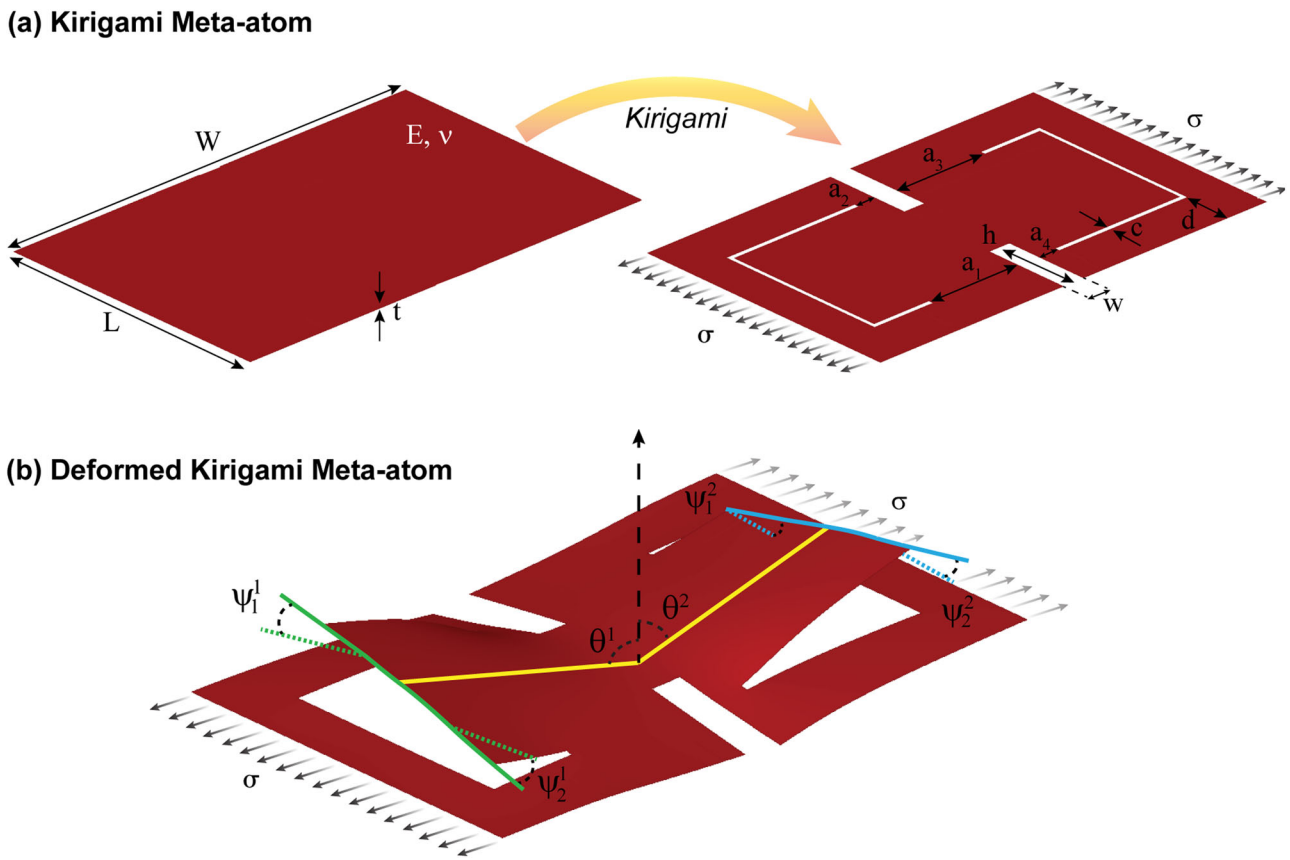

Fig. 1 Kirigami meta-atom template. a Initial Kirigami canvas and canvas with interior cuts. **b** Deformed Kirigami with relevant deformation descriptors.

(*features*), linear and geometrically-nonlinear finite element analyses are conducted to solve the linear and nonlinear buckling problem, respectively. While the former provides the necessary imperfection modes to trigger the bifurcations in the system, the latter provides the deformation and structural metrics that define the target properties of our design problem (*responses*). Specifically, the deformed coordinates of the centerline traversing the inner panels and of the two lateral edges of each panel are chosen as representative of the deformed configuration of the Kirigami meta-atom (Fig. 1b). Far from being complete descriptors of the Kirigami deformations, these coordinates are sufficient to describe the three-dimensional rotations of the panels (tilts, θ_{1-2}, and twists, ψ_{1-2}^{1-2}) necessary for various applications. Similarly, the force-displacement curve is obtained from simulations as indicative of the structural response of the Kirigami. Together with the geometric parameters of the underformed configurations, the deformation and structural metrics constitute the dataset. The dataset is subsequently fed to our machine learning framework, which rests on three pillars that contribute to the rational design of the Kirigami. The first one uses a clustering approach to explore the space of achievable deformed configurations (i.e., what shapes are possible?). The second one leverages a tandem deep neural network (T-DNN) architecture to predict the cut layout to obtain a specific deformed configuration (i.e., how should the Kirigami be cut?). The third and final approach uses symbolic regression to obtain surrogate models that predict variables relevant to the tunable actuation of the designed Kirigami meta-atom (i.e., what is the range of accessible deformation?). All combined, these approaches provide an unequivocal picture of the Kirigami meta-atom which, when supplemented with integrative elements (e.g, array architecture/actuation, surface functionalization), can guide the design of functional Kirigami metamaterials. The framework is summarized in Fig. 2.

RESULTS AND DISCUSSION

Characterization of the Kirigami design space

We begin the design endeavor by characterizing the limits of achievable Kirigami configurations for a set of cut geometries. This is essential to future steps along the design process (e.g., optimization, implementation, etc). In terms of the Kirigami design problem here advanced, this translates into a need for knowing what basic 3D out-of-plane deformations are attainable leveraging the proposed Kirigami motif. In the past, a number of authors have attempted to map the Kirigami landscape of the present motif, but they have done so under consideration of a subset of possible cut geometries (e.g., by changes in hinges lengths, symmetric layouts, etc.)[7,8,19]. As such, these prior investigations provided a limited description of Kirigami-based potential designs. With the purpose of elucidating the full Kirigami design landscape, we proceeded to comprehensively survey the range of deformed configurations from sampling variations involving all ten of the geometric parameters defining the cut layout $\{a_{1-4}, h_{1-2}, w_{1-2}, c_{1-2}\}$. Using linear buckling FEM simulations, the out-of-plane deformations corresponding to each combination of cuts was characterized and fitted, using a 5-knot B-spline, to the deformed coordinates of the centerline traversing the inner panels (Fig. 3a). The five-coefficient vector, representative of the deformation, was subsequently reduced to two representative principal components (PCs) using singular value decomposition (SVD). The dimensionally reduced data, capturing over 98% of the variance of the original dataset, was further processed using k-means clustering. This enabled partition of the space of Kirigami deformations into five well-defined representative clusters (Fig. 3b–f). As expected from previous studies, symmetric and asymmetric linear ($/, \backslash$) and nonlinear shapes ($\cup, \cap$) with their mirror images represent 4/5 of the total space (Fig. 3b–e). Furthermore, a cluster situated midways from the others, is

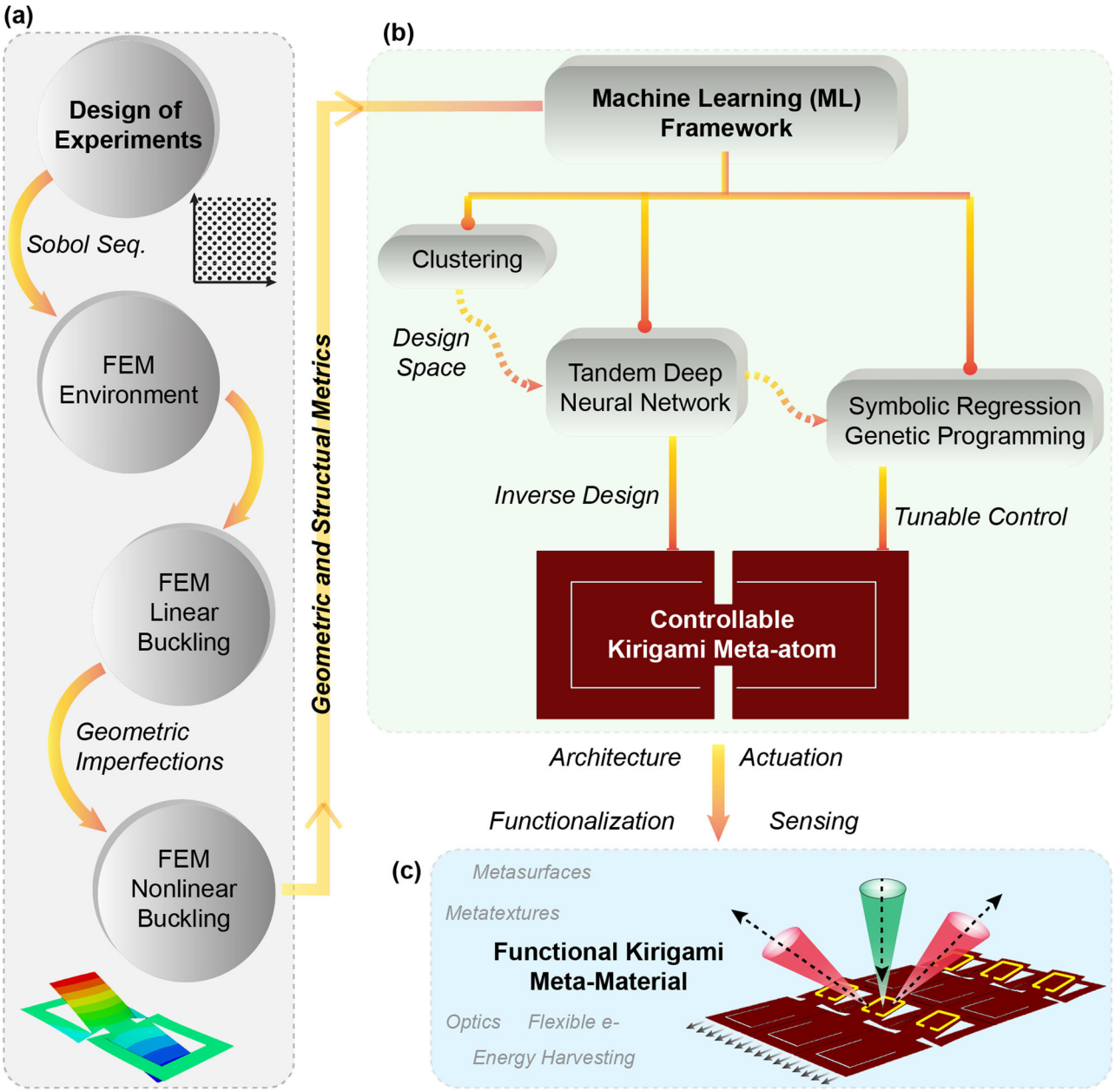

Fig. 2 General framework for the machine learning assisted design of Kirigami meta-atoms and metamaterials. a Dataset collection. **b** Machine learning framework. **c** Implementation of Kirigami machine learning design.

identified, which contains an array of miscellaneous shapes that not only present symmetric and asymmetric features but also exhibit local minima and maxima (Fig. 3f). As such, the value of the clustering analysis lies in its capacity to provide an overall picture of the versatility of a given Kirigami motif. With the configurational space ascertained, one can infer that the present motif is suitable for a variety of applications, e.g., flat mirrors (using clusters c-d), solar troughs (using clusters b-e), or even free-form optics (using cluster f), to name a few. Moreover, the knowledge and visualization of the different unique shapes of the deformed configurations of the Kirigami motif unfolded by the clustering allows the designer to come up with a way to uniformly characterize the deformed configuration using measures like tilt and twist angles. Having identified the aptness of the Kirigami motif to design problems of practical relevance, we next introduce a deep neural network approach to obtain the specific set of cut parameters that would fulfill a particular quantitative design requirement.

Inverse design of the Kirigami meta-atom

In the realm of Kirigami-based metamaterials, the inverse design of Kirigami has essentially been achieved by the use of constrained optimization techniques[9,11]. Although Kirigami layouts obtained by such schemes are highly accurate (i.e., meeting the intended target), the process itself can be time intensive. For each new target shape, the entire design space has to be searched again, which can lead to the need for carrying out hundreds to thousands of numerical simulations in every iteration. In sharp contrast, in data-driven approaches like neural networks, the complete training dataset is obtained by carrying out the entire batch of simulations once. Therefore, a neural network-based framework for inverse design can reduce the computational effort spent on expensive numerical simulations required for multiple design tasks.

To tackle the challenge of designing Kirigami meta-atoms geared towards achieving a specific deformed configuration, we

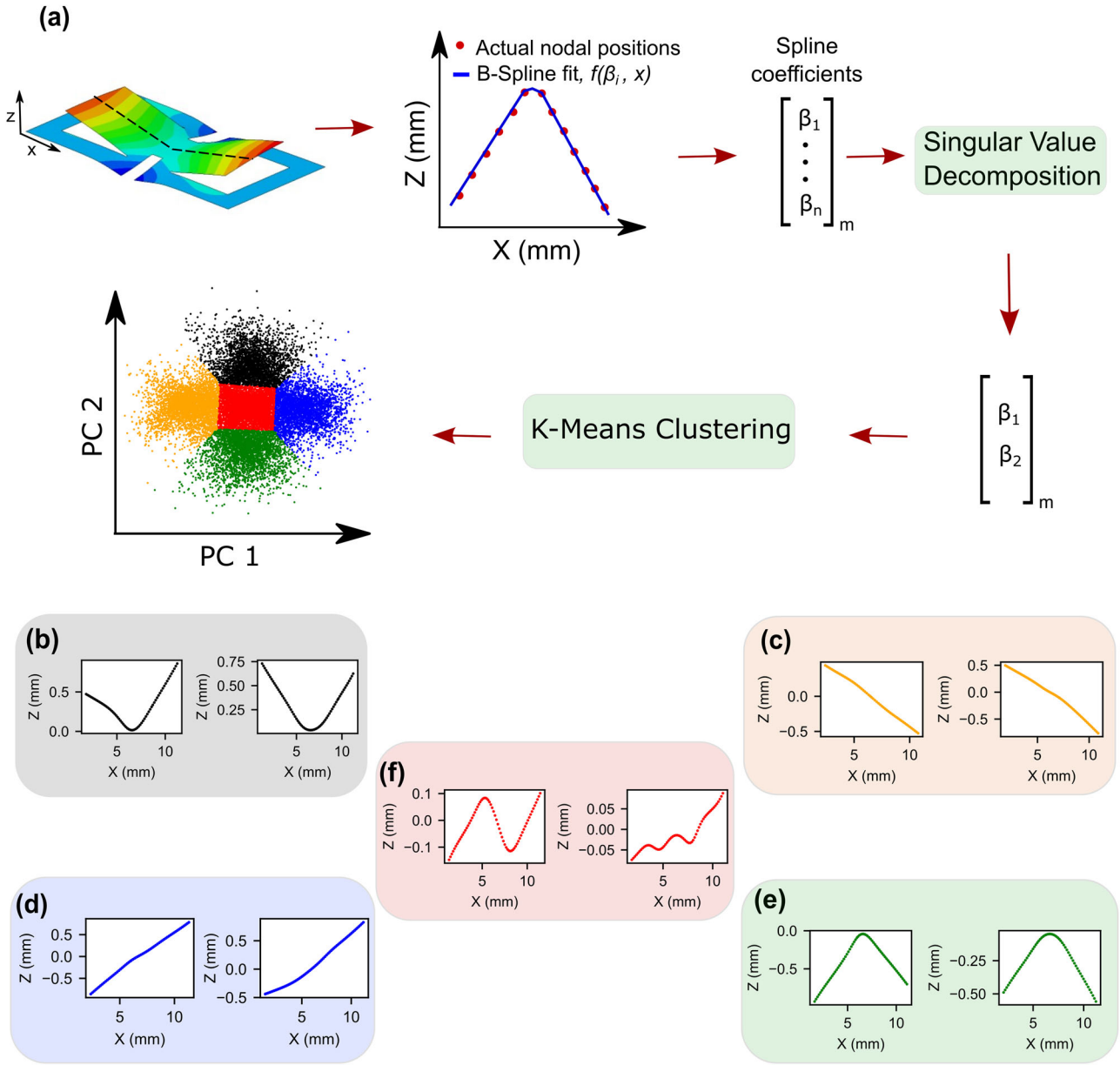

Fig. 3 K-means clustering based on the final z-coordinates of the nodes along the centerline of the Kirigami meta-atom. a Data processing workflow for clustering the models based on the deformed shape of the inner panels. Five different clusters were produced by k-Means clustering of the principal components of the B-spline coefficients fitted to the z-coordinates. **b**–**f** Representative examples of the final shapes of the centerline of the central panel for the black, yellow, blue, green, and red clusters, respectively shown in the scatter plot in **a**.

leverage a machine learning-based inverse design strategy. Specifically, we employ a tandem neural network architecture[13,20], comprised of a forward (*f-NN*) and an inverse (*i-NN*) deep neural network (Fig. 4a). As proof-of-concept and without loss of generality, the ML-based inverse design approach is conducted for the same Kirigami motif, but considering only variations in the length of the hinges (geometric parameters a_{1-4}).

In the first step, we train the *f-NN* to predict the parameters that define the deformed configuration ($\theta_{1-2}, \psi_{1-2}^{1-2}$, Fig. 1) stemming from a given meta-atom cut geometry (a_{1-4}). As such, the fully trained *f-NN* accurately (coefficient of determination $R^2 \sim 0.93-0.94$) relates the planar cuts to the 3D deformations on a test set, hence constituting an inexpensive emulator for the otherwise costly FEM simulations (Supplementary Note 1 and Supplementary Figure 2a–f).

Unlike the *f-NN* mapping, the inverse problem of predicting the design parameters (cut geometry) for a specific deformed configuration is not well-posed due to the fact that a multiplicity of Kirigami meta-atom designs can lead to the same deformed configuration (i.e., non-unique solution). This non-uniqueness is inherent to most inverse design problems and often leads to convergence issues when training a neural network on such a dataset[13,21]. To circumvent this issue, we complement the forward mapping with an inverse mapping in a tandem fashion with a modified loss function that incorporates two loss terms. The first one, a direct-loss term representing the difference between the *i-NN* predicted design parameters and the actual design parameters; whereas the second one, the reconstruction-loss term, quantifies the difference between the desired deformation angles and the *f-NN* or FEM reconstructed

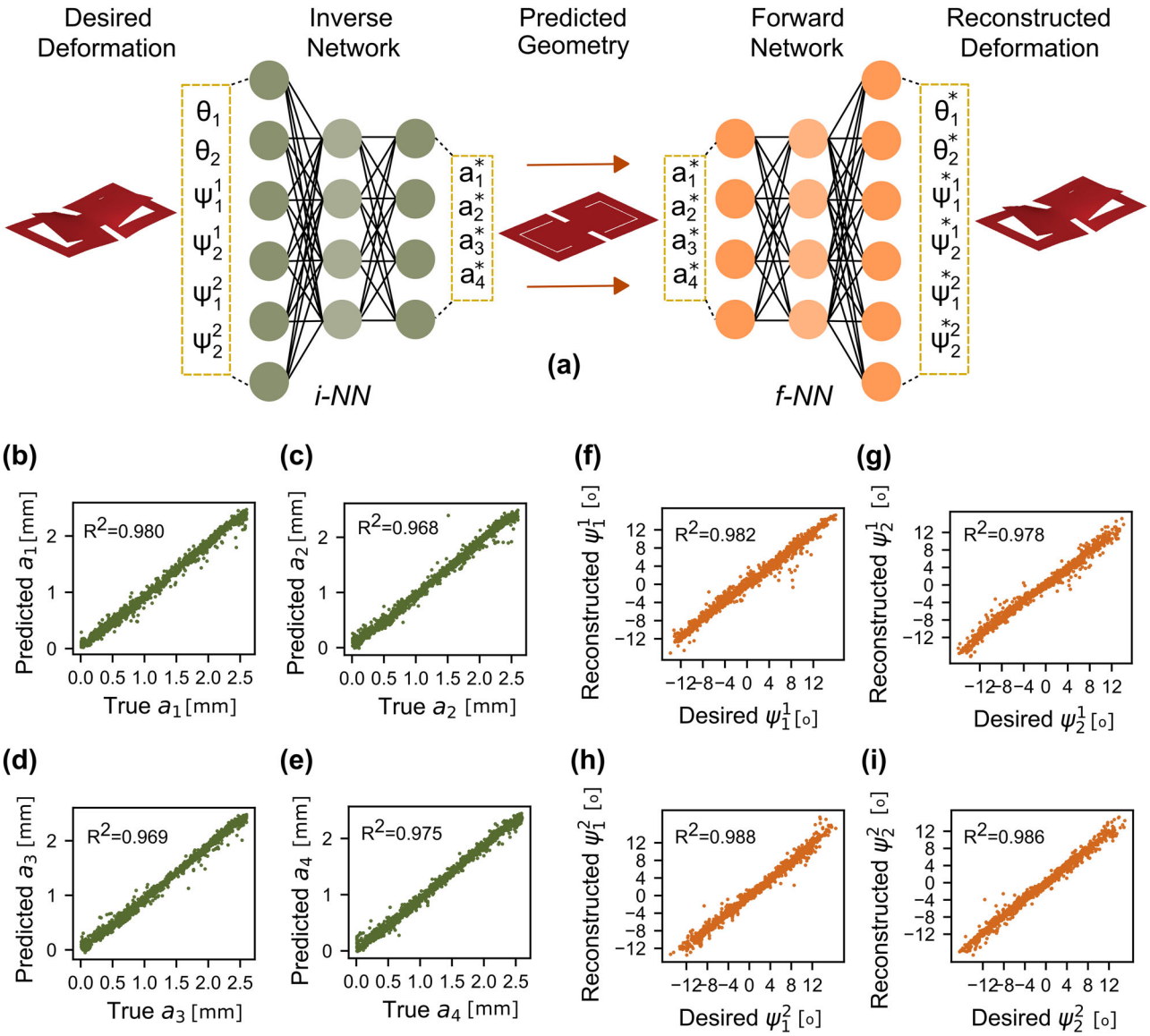

Fig. 4 Machine learning framework for inverse design. a Schematic of the tandem network architecture employed for the inverse design. The inverse network (*i-NN*) takes in the desired deformed configuration $(\theta_{1-2}, \psi_{1-2}^{1-2})$ and predicts a set of geometric features (a_{1-4}^*). The *i-NN* predicted geometric features (a_{1-4}^*) are fed to the pretrained *f-NN* to reconstruct the angles of the deformed configuration $(\theta_{1-2}^*, \psi_{1-2}^{*1-2})$ and thereafter validate the predictions of the *i-NN*. **b**–**e** *i-NN* predicted a_{1-4} vs true a_{1-4}. **f**–**i** *f-NN* reconstructed ψ_{1-2}^{1-2} vs desired ψ_{1-2}^{1-2}. The corresponding coefficient of determination (R^2) are specified on the respective plots.

deformation angles (Eq. 1), viz.:

$$Loss_{i-NN} = \frac{1}{n}\sum_{i=1}^{n}\lambda\|g(\mathbf{\Theta}) - \mathbf{a}\|^2 + \frac{1}{n}\sum_{i=1}^{n}\mu\|f(g(\mathbf{\Theta})) - \mathbf{\Theta}\|^2 \quad (1)$$

where g $(\mathbf{\Theta})$ inverse mapping, f $(\mathbf{a})$: pretrained forward mapping, $\mathbf{a} = [a_i]$ and

$$\mathbf{\Theta} = \left[\theta_k, \psi_k^l\right], \lambda \, and \, \mu > 0.$$

The incorporation of the direct-loss (first term in Eq. 1) ensures that the predicted design parameters are constrained to be within a physically meaningful range without deviating too far from the true values. Conversely, minimization of the reconstruction-loss, which uses the pretrained *f-NN*, ensures that the *i-NN* predicted design parameters lead to the desired deformed configuration. In other words, the reconstruction-loss ensures that for the cases where there are multiple sets of design parameters (a_{1-4}) for the same design requirement $(\theta_{1-2}, \psi_{1-2}^{1-2})$, every set yields positive training feedback. The values of the scalars λ and μ set the weights of the respective loss terms.

To evaluate the fully trained *i-NN* we used the test set. For every set of desired deformed configuration $(\theta_{1-2}, \psi_{1-2}^{1-2})$, the *i-NN* predicts the candidate set of design parameters (a_{1-4}^*) that is likely to yield the desired deformation. The design validation is performed by feeding the a_{1-4}^* to the pretrained *f-NN* to reconstruct the deformation angles $(\theta_{1-2}^*, \psi_{1-2}^{*1-2})$ that a Kirigami meta-atom with a_{1-4}^* as its design parameters would yield. The reconstructed set $(\theta_{1-2}^*, \psi_{1-2}^{*1-2})$ is finally compared to the desired set $(\theta_{1-2}, \psi_{1-2}^{1-2})$. A few representative examples comparing the reconstructed set to the desired set of deformation angles from a test dataset are shown in Fig. 4f–i. The coefficient of determination, R^2, was around 0.98 between all the desired angles and the reconstructed angles of the deformed state of the Kirigami meta-atoms. In addition, we also show that the *i-NN* predicts the design parameters (a_{1-4}) well for all the cases in the test set ($R^2 = 0.96 - 0.98$, Fig. 4b–e).

As such, the T-DNN framework enables a computationally efficient methodology to design Kirigami meta-atoms with specific deformation-based design requirements, which can be easily modified to accommodate other Kirigami meta-atom designs and design objectives. However, an important point to be noted is that neural network-based design frameworks cannot outperform iterative methods of optimization in terms of accuracy. This is because data-driven approaches like neural networks (NNs) always have an error associated with them as data-driven methods are merely emulators of the real process. In the absence of computational time constraints, traditional optimization techniques can arrive at the desired solution with better accuracy. Therefore, if the application involves only a few design tasks, standard optimization techniques can work equally well. As the design space grows, NNs offer the advantage of speed. Another possibility could be the use of NNs to obtain a first estimate of the solution, followed by application of conventional iterative optimization schemes to converge to the design target.

Tunable control of the Kirigami meta-atoms

The Kirigami motif obtained via the T-DNN strategy satisfies the deformation criteria when subject to a fixed stretch level. In this sense, the obtained deformation parameters constitute a sort of intermediate bound along the deformation path of the rotating panels following bifurcation. While this approach aptly satisfies designs that require a fixed level of deformation for functionality (e.g., a deployable flat mirror always oriented at θ degrees), it leaves aside the possibility of tuning the deformation to encompass a range of deformed states (i.e., tunable deformation control). To address this matter, we seek parsimonious models that relate the geometries of the cuts to parameters relevant to the tunable control of the Kirigami via nonlinear symbolic regression by genetic programming. Such an approach not only complements the inverse-design process but also augments the virtues of the designed meta-atom.

To illustrate the framework, we focus on characterizing the bifurcation diagram of the Kirigami panels, i.e., the actuating force to the panel tilt ($F-\theta$). First, a symbolic expression for the critical tensile force (F_{crit}) that gives rise to the out-of-plane displacement of the inner panels ($F_{\text{crit}} \approx f(a_{1-4})$) is obtained (Fig. 5a, i). Knowledge of the critical buckling force provides a first coordinate pair ($\theta = 0, F = F_{\text{crit}}$) for the subsequent reconstruction of the bifurcation curve. Using the values of the critical force obtained from the FEM simulations previously described, we obtained the following best 5-genes parsimonious model (Fig. 5a, ii-iii), with an $R^2 \approx 0.95$ (test set), viz.,

$$\begin{aligned} F_{\text{crit}} = {} & 0.018a_1^{1/2}(a_3+a_4) + 0.014a_2(a_4+a_3^{1/2}) - 0.0035a_1a_2^2 \\ & - 0.0004(a_3+3a_4)(a_3+a_1^{\frac{1}{2}})(a_3+2a_4) \\ & + 0.002a_1a_3(a_4+2) + 0.14 \end{aligned} \tag{2}$$

Next, employing two coordinate pairs ($\theta = 0, F = F_{\text{crit}}$, and $\theta = \theta_1, F = F_{\max}$) the bifurcation diagrams (Fig. 5b, i) of each Kirigami are fitted assuming a quadratic relationship (i.e, $F \approx k\theta^2 + F_{\text{crit}}$, vertex form), where the leading term (k) is subsequently modeled against the geometries of the cuts ($k \approx g(a_{1-4})$, Fig. 5b, ii-iii). The assumption of the quadratic relationship to describe the progression of the deformation is based on the nature of the physical phenomena (pitchfork bifurcations). Using symbolic regression, the best 5-genes parsimonious model, with an $R^2 \approx 0.93$ (test set), is:

$$\begin{aligned} k = {} & \left[6.46e^{a_1} + 5.09e^{a_2}\tanh a_2^2 + 9.28e^{a_1}\tanh(a_2a_3) + 9.33e^{a_2}\tanh(a_1a_4)\tanh a_2 \right. \\ & \left. - 3.84a_1a_2a_3a_4\tanh(a_3a_4) - 8.5\right]x10^{-4} \end{aligned} \tag{3}$$

Combining the two surrogate models, the Kirigami designer can construct response diagrams or integrate these expressions in a control logic, that would enable precise operation of the Kirigami meta-atom (*Kixels*) at a variety of actuation levels, thus circumventing the need for additional FEM simulations with the added simplicity of easily programmable free-form and closed-form expressions. Going back to the example of the deployable mirror/tracker, the designed Kirigami can now be precisely actuated to reflect/collect light at various angles depending on the position of the light source (Fig. 5c). Noteworthy, the nature of the solution obtained, as in every symbolic regression problem, depends on the set of basis functions used (akin to how neural networks depend on activation functions). With that in mind, we have sought to use a broad class of mathematical functions to avoid biasing and limiting the final expression. Without pursuing derivation of universal law, the solutions found (accurate and limited in expressional complexity), fulfill the very pragmatic purpose of assisting the Kirigami engineer in controlling and tuning its design. Similarly, while the above-obtained relationships lack physical insight and are dependent on the unit system of the original dataset, they constitute an accurate and effective way to individually control the designed meta-atom, which is of great importance when coupled with distributed actuation (i.e., control at the *Kixel* level). With the aid of dimensional analysis, namely grouping of parameters by the Buckingham π-Theorem, together with larger and more encompassing material and geometric datasets, physically meaningful and general laws could be extracted to model the response of Kirigami. As an example, the critical buckling force is discussed in Supplementary Note 2.

From meta-atoms to metamaterial applications

The proposed data-driven design framework can be applied to the design of Kirigami metamaterials or structures by combining arrays of Kirigami meta-atoms. At this higher hierarchy level, functionality is achieved by complementing the direct functionality (i.e., 3D out-of-plane deformations of the panels) with elements pertaining to the architecture (i.e., spatial disposition of meta-atoms), actuation (e.g., single/distributed/smart actuation), and the functionalization of the active surface (e.g., coatings, embedded electronics for sensing, sub-textures, etc.). While every particular application requires an adequate, ad-hoc dataset (e.g., training for tilts and twists may not be ideal for designing Kirigami with prescribed curvatures), the framework here introduced is general enough to illustrate its potential through a variety of applications that have bio-inspiration as a common guiding principle.

To illustrate this, we start at the meta-atom level. Figure 6 presents the inverse design and experimental validation of three Kirigami motifs with proof-of-concept design conditions. The experimental validation consisted of (i) patterning the machine learning predicted motifs using a laser cutter, (ii) subjecting the Kirigami specimens to uniaxial stretch, while recording its structural response (Force-Displacement curves), and (iii) obtaining the out-of-plane displacements of the panels (u_z) using the classical Shadow Moiré technique. The first two examples respond to design requirements where overall linear shapes with a fixed slope (tilt) are preferred but with varying requirements with respect to the twist of the panels (untwisted and twisted, respectively). These objectives could easily typify design conditions for light modulation and three-dimensional light steering using flat mirrors. The third example corresponds to a design objective of an overall nonlinear shape with symmetric tilts, which could be representative of a mechanical gripper design with a maximum contact angle. As can be seen from Fig. 6, there is good agreement between the prescribed design objectives and the experimental observations of the different tilts and twists. Furthermore, the critical forces predicted by the symbolic regression approach are also in accord with the experimental observations of the inflection points in the meta-atom's structural

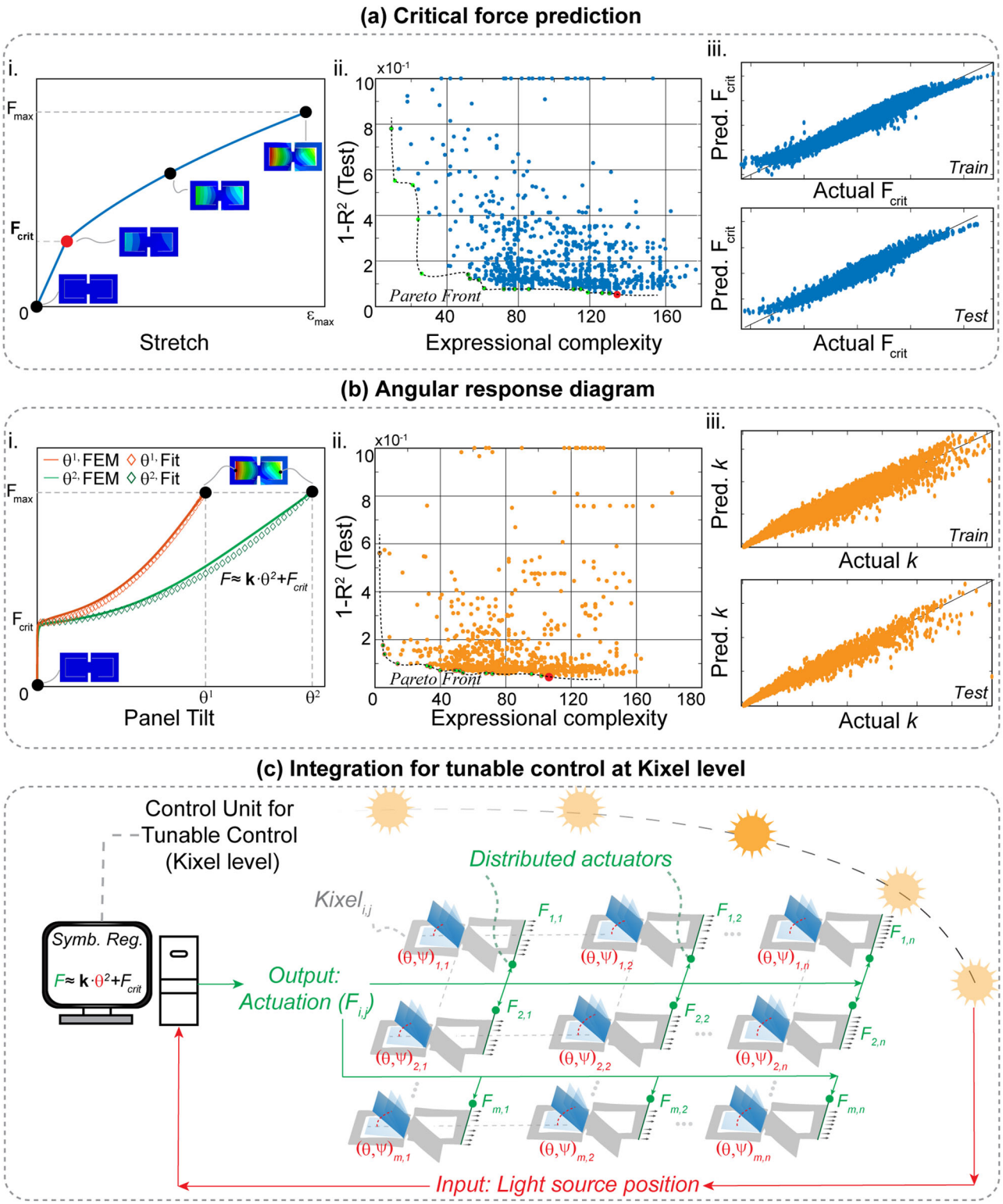

Fig. 5 **Symbolic regression for control of inversely designed Kirigami meta-atoms. a** SR applied to structural response of Kirigami: (i) Force-displacement relationship, (ii) Accuracy vs. complexity of parsimonious mode with pareto front defined by green points, (iii) Predicted vs. actual critical force for training and test set. **b** SR applied to structural response of each panel: (i) FEM and fitted bifurcation curves, (ii) Accuracy vs. complexity of parsimonious mode with pareto front defined by green points, (iii) Predicted vs. actual fitting constant *k* for training and test sets. **c** Schematic diagram for application of the symbolic regression framework for tunable control of Kirigami units with distributed actuation.

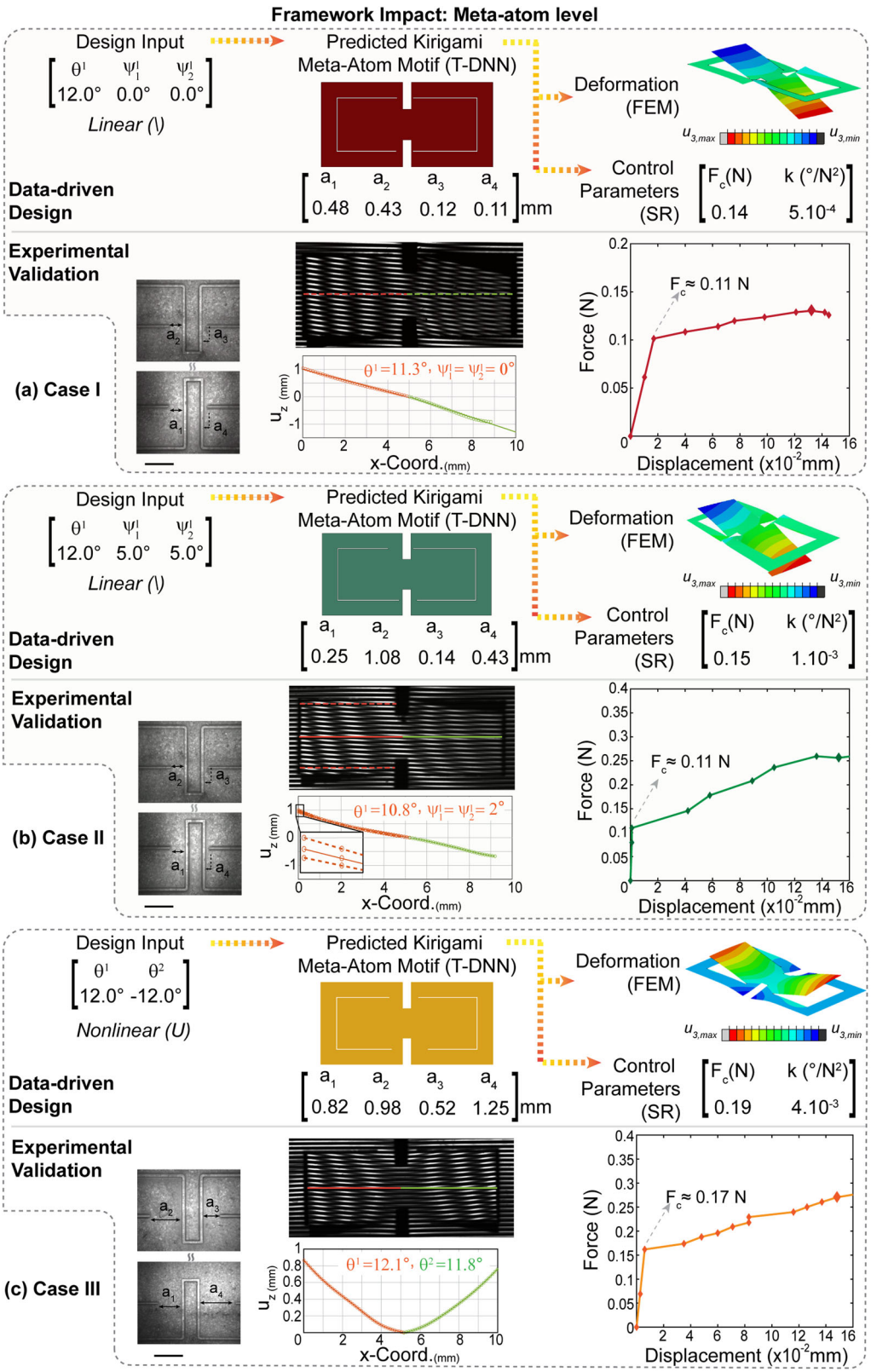

Fig. 6 Inverse design framework application and experimental validation at the meta-atom level. a Design case I (Linear kirigami without twist). **b** Design case II (linear kirigami with a twist). **c** Design case III (nonlinear kirigami). Scale bar = 1 mm.

response. Differences between expected and observed results can arise from a variety of sources, which fundamentally stem from the fact that the derived physics-based surrogate model has been trained on models that may not incorporate all the variables and uncertainties of the problem. As such, we hypothesize that the omission of higher order imperfection modes (and their interactions), together with the exclusion of the material's plastic behavior (i.e., hinges act as stress concentrators, which may

locally yield), and the imperfections from the manufacturing process (e.g., local charring, geometric deviations from prescribed design, residual stresses/deformations that influence buckling imperfections, etc.) are most likely to be accountable for the discrepancies. While presently out of the scope of this paper, quantification and introduction of the aforementioned variables (i.e., uncertainties) in data-based design frameworks (e.g., probabilistic and/or Bayesian machine learning[12,22]) will be paramount when striving for reliable buckling-based shape-morphable Kirigami devices operating in the field.

At the metamaterial level, Fig. 7 conceptually and experimentally illustrates the use of the abovementioned Kirigami on four bioinspired 1D and 2D metamaterial designs. The first, inspired by the hairy structures found on the Western Honey Bees (*Apis mellifera*), known to trap pollen particles[23], consists of a Kirigami metatexture comprised of meta-atoms in series, exhibiting in-plane actuation and symmetric tilts ($\theta_{1-2} \leq 12^{\circ}$). Such design is envisioned for the entrapment of particles of different sizes (angle-stretch tunability) (Fig. 7a and Supplementary Video 1). Another Kirigami metatexture design is envisaged, this time inspired by the protruding barbs of the Bunny-Ear cacti (*Opuntia microdasys*), which facilitate droplet transport and collection[24]. Mimicking the natural counterpart, the metatexture leverages in-series arrays of linear and flat Kirigami arranged in a triangular fashion and actuated at an angle (Fig. 7b and Supplementary Video 2). Since only a single protruding panel is of interest, the base design condition for this case becomes $\theta_1 \leq 12^{\circ}, \psi^1_{1-2} = 0$. For the third metamaterial, we chose to highlight the versatility of Kirigami-engineering, by trying to mimic the heliotropic motion of daisies (*Bellis perennis*). In this case, a standard solar-tracking requirement would be to allow for high tilt angles ($\geq 45^{\circ}$). Given that our sampled design space, only allows for maximum tilts of ($\theta \approx 20^{\circ}$), new designs had to be sought. Without generating new data and/or training new networks, we started with a machine learning design of linear Kirigami meta-atoms, and then, using mechanical- and Kirigami-design intuition, we first tuned the length of the hinges (to symmetrize displacements) followed by adjustment of the width of the vertical U-Cuts (to obtain extreme tilts). Following this heuristic strategy, a Kirigami meta-atom, actuated at the same level as our base Kirigami, yielded extreme tilts. We note that an automated and computationally efficient procedure is possible when using adaptive learning strategies[25]. Structuring the obtained meta-atom in 1D and 2D arrays, a solar-tracking metatexture can be arrived at (Fig. 7c and Supplementary Video 3). Finally, another thought-provoking bioinspired design is motivated by the mirror-eyes of the Bay Scallop (*Argopecten irradians)*, which exhibit parabolic surfaces that reflect incoming light onto the retina[26]. To emulate such extraordinary design, Kirigami meta-atoms that deform into parabolic surfaces are sought. We note that for the limited set of geometric cut parameters varied in the inverse design framework previously discussed, only V-shaped deformations and not parabolic ones can be obtained. To address this matter and obtain parabolic configurations, we follow a similar machine learning assisted approach (as for the solar tracker), complementing our ML-framework approximation by tuning the vertical cuts (defined by h, w) and the width of the inner cuts (defined by c). Using this strategy, which highlights the power and versatility of Kirigami-engineering and of the developed framework, a Kirigami strip actuated into a dome with *local* parabolic shapes was obtained. Here, hoop strains induce the stretch necessary to trigger the panels' bifurcations, see Fig. 7d. This reflector, made of parabolic Kirigami, with tunable *foci*, could be leveraged to focus light similarly to the eye of the bay scallop. Realization of this type of smart surfaces could be achieved by means of pneumatic actuation, where an array of carefully aligned nozzles (or an airblade) propel a sheet-like stream of air onto the exterior surfaces (i.e., sidebands outside the C-cuts) of the Kirigami strip. Though the implementation details are presently outside the scope of this work, we hope the presented examples inspire the use of programmable and tunable Kirigami in the very active field of flexible optics and imagers. Noteworthy, the mechanical-intuition-based complementary step could be replaced by a more efficient standard topology optimization step, where the T-DNN solution is leveraged as an initial guess or starting point. While the proposed framework was validated with arrays of Kirigami with the same motif, a combination of motifs from the same or different clusters is possible. Whereas design and applications of combined surfaces within the same cluster has been demonstrated for the case of a linear Fresnel mirror in previous work by ref. [8], the interaction of meta-atoms and functionality of surfaces, combining linear and nonlinear deformation-shapes, should be further investigated.

Beyond bioinspired metasurfaces, our framework can also be employed in the design of more complex metamaterials, in a variety of physical problems. One of such possibilities, is presented by the field of optical metasurfaces, where structural reconfigurability, coupled with passive elements (e.g., resonators that change orientation with respect to an incoming field) could be exploited to modify the electromagnetic response of the material[27]. In the field of mechanical metamaterials, clever combinations of the Kirigami motif here investigated could be used for programmable elastic wave propagation control and for friction/drag control aimed at energy dissipation. While the complexities of each application merit individual studies, and proper selection of NN output variables, we expect the introduced framework to accelerate the use of Kirigami-engineering in such applications.

The aforementioned applications make a formidable case for both the power and versatility of Kirigami-engineering as well as for the need for data-driven frameworks, like the one proposed here, to accelerate the design process in the face of rich design spaces.

To summarize, Kirigami-engineering has been hailed as a game changer in the field of reconfigurable metamaterials, but its current development points to a potential that is yet to be fully realized. In no small measure, responsible for the shortcomings of Kirigami-engineering are the difficulties associated with their rational design, which stem from their inherent nonlinearity, the lack of analytical models, and their vast design and response spaces. In an attempt to bring Kirigami-engineering closer to its true potential, we have here introduced a comprehensive data-driven framework that not only addresses the inverse design of Kirigami but also provides utilitarian means to aid in their control and take advantage of Kirigami's tunability. While exploring a relatively limited design space, the application of the proposed framework to inform the design of bioinspired metamaterials, over a range of hierarchal levels reveals the value of the reported approach in the face of complex Kirigami applications.

For future exploration, a much broader set of cut geometries and patterns can be incorporated, which could potentially be addressed by the T-DNN framework shown here with certain modifications to the network architecture and hyperparameters or by other inverse design algorithms like supervised autoencoders[15] and variational autoencoder[28]. The anticipated increase in the dimensionality of the problem can be tackled by incorporating convolutional neural networks (CNN), wherein the entire image of the Kirigami motif (which inherently includes all the geometric parameters) could be used as an input to the CNN that maps the geometry to the deformed configuration via a lower dimensional fully connected neural network. Moreover, to facilitate designing for deformation parameters that are not within the initial training design space, techniques like active transfer learning and data augmentation can be employed[25]. Additionally, material properties, initial geometric imperfections, distributed actuation, and associated uncertainties pose a vista of opportunities and

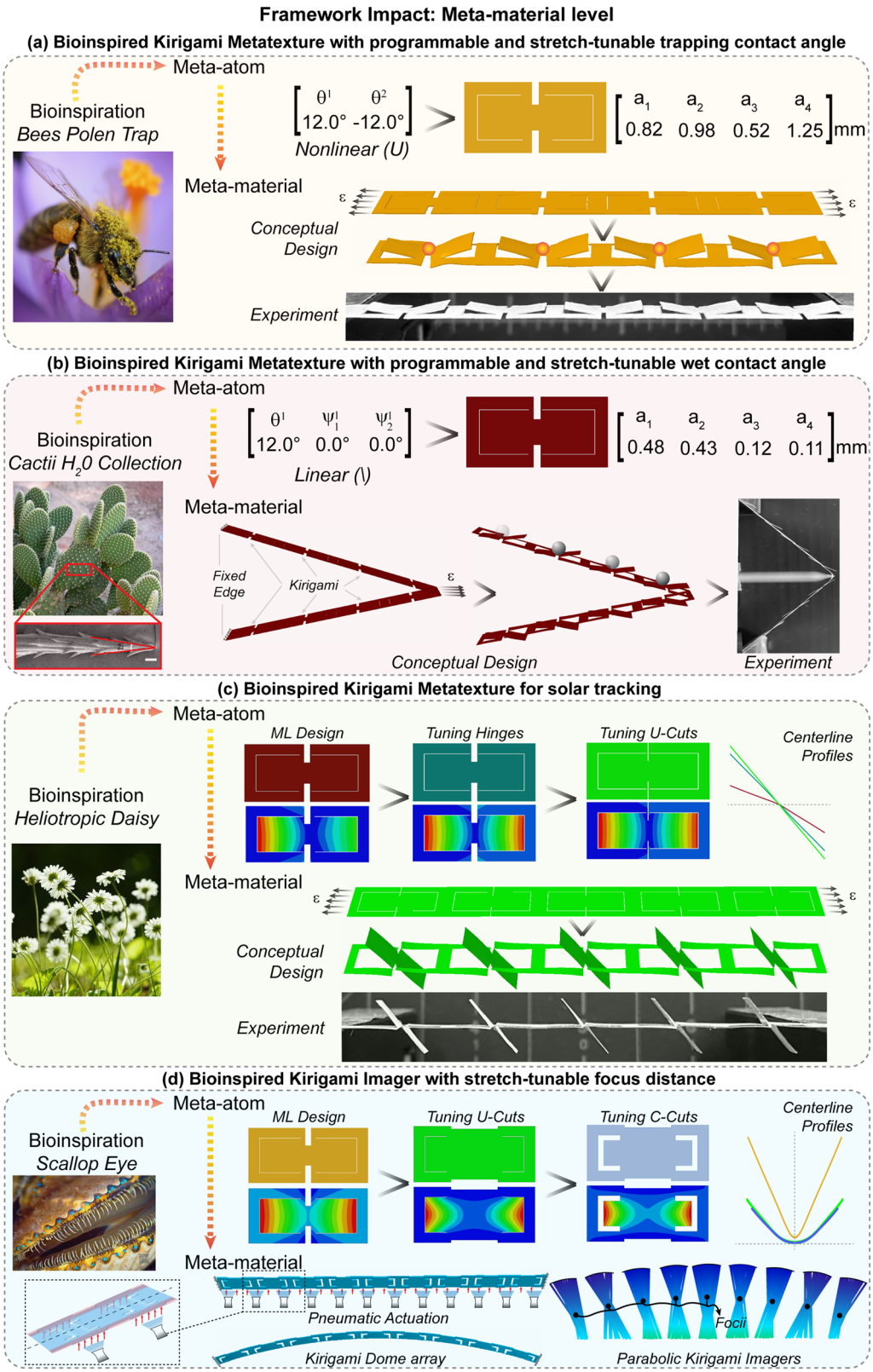

Fig. 7 Inverse design framework application and experimental validation at the metamaterial level. Photo credit: **a** Kirigami metatexture for tunable trapping. Photo of bee courtesy of Annette Meyer. **b** Kirigami metatexture for tunable wet contact angle. Optical photography by Stan Shebs, under CC BY-SA 3.0 license, and SEM micrograph adapted from ref. [24]. **c** Kirigami metatexture for solar tracking. Photo of daisies courtesy of jhening. **d** Kirigami metatexture for flexible imagers. Photo of scallop courtesy of David Moynahan Photography. All pictures were used with permission from the authors or under an appropriate license.

challenges for future work, that will undoubtedly propel the intelligent design of Kirigami and mechanical metamaterials. With reliability and robustness of Kirigami devices in mind, the use of full-field techniques (e.g., 3D-DIC) could be used to identify regions undergoing plasticity or strain localization, which may negatively impact functionality. As such, we envision future Kirigami designers using and drawing inspiration from our approach as a platform to realize multifunctional Kirigami metamaterials operating at the nano-, micro-, and macroscale.

METHODS

Sobol sampling

For the k-means clustering analysis, geometric parameters defining the inner cuts $\{a_{1-4}, h_{1-2}, w_{1-2}, c_{1-2}\}$ were obtained from a quasi-random Sobol sampling using $N = 20000$ sample points, $n_{var} = 10$ decision variables. For the NN inverse design and symbolic regression, geometric parameters defining the Kirigami hinges (a_1, a_2, a_3, a_4) were obtained from a quasi-random Sobol sampling using $N = 15000$ sample points, $n_{var} = 4$ decision variables. All sets were obtained, randomly linearly scrambled, and digitally shifted using MATLAB R2020 (MathWorks, Natick, MA, USA). Lower and upper bounds for the decision variables were chosen as: $\{0.0065\,\text{mm}; 2.6\,\text{mm}\}$.

FEM Simulations

All simulations were carried out using ABAQUS/STANDARD and ABAQUS/CAE 2020. The linear eigenvalue buckling under global tension was solved using the Lanczos algorithm implemented in Abaqus (*BUCKLE, EIGENSOLVER = LANCZOS). The first buckling eigenmode was extracted and used as initial geometric imperfection for the subsequent nonlinear geometric analysis (Supplementary Note 3). The post-buckling analysis was conducted using a nonlinear geometric step (*NLGEOM) with numerical integration parameters: maximum number of allowed increments ($N_{incr} = 10^4$), initial time step ($\Delta S_0 = 10^{-4}$), minimum time step ($\Delta S_{min} = 10^{-10}$), and maximum time step ($\Delta S_{max} = 10^{-3}$). Following mesh convergence analysis, the Kirigami geometry was meshed using three-dimensional, finite strain, first order quadrilateral shell elements with reduced integration (Abaqus elements S4R), with a size of $\Delta l = 0.01$ mm. One of the vertical edges of the Kirigami meta-atom was fully constrained, while the opposite edge was subject to a uniaxial displacement ($\Delta x/t = 1.5\%$). The material properties of Kapton tape were used as a reference for all the models ($E = 2.5$ GPa, $\nu = 0.34$). For the clustering analysis, fixed geometric dimensions were (all in mm): $L = 13$, $W = 6.5$, $t = 0.065$ and $\delta = 1.17$. For the inverse design analysis, and symbolic regression, fixed geometric dimensions were (all in mm): $L = 13$, $W = 6.5$, $t = 0.065$, $h_{1-2} = 2.07$, $w_{1-2} = 0.65$,$\delta = 1.17$, $c = 0.065$. Critical buckling forces for symbolic regression were extracted from the linear buckling models. Tilts of the inner panels (θ_{1-2}) were computed from the final coordinates of the nodes along the centerline of the Kirigami. Similarly, twists of the inner panels (ψ^1_{1-2}) were computed from the final coordinates of the nodes along the lateral chords of the panels. A python script was used to automate the preprocessing, processing, and post-processing stages of the FEM models.

Forward neural network

A threefold cross-validation method was employed to segregate the ground truth data (15,000 models), obtained via FEM simulations, and then train and validate the model. A deep neural network architecture with three hidden layers (Supplementary Note 1 and Supplementary Table 1) was trained to minimize the mean squared error loss between the true deformation angles $(\theta_{1-2}, \psi^{1-2}_{1-2})$ and the ones predicted by the *f-NN*, with respect to the weights and biases of the *f-NN*.

$$\text{Loss}_{f-NN} = \frac{1}{n}\sum_{i=1}^{n} ||f(\mathbf{a}) - \mathbf{\Theta}||^2 \tag{4}$$

where f (**a**): forward mapping, $\mathbf{a} = [a_i]$ and $\Theta = \left[\theta_k, \psi^l_k\right]$

During the optimization, the weights and biases of the *f-NN* were updated using a backpropagation algorithm available in the PyTorch library[29].

Inverse neural network

A deep neural network architecture with two hidden layers (Supplementary Note 1 and Supplementary Table 1) was used. Model training and validation was carried out using a threefold cross-validation method. The values of μ, λ used during the final training (Supplementary Note 1 and Supplementary Table 1) were determined based on ease of convergence and prediction accuracy using a grid search approach.

Symbolic regression

Symbolic regression via genetic programming models were implemented using the MATLAB-based open-source software of GPTIPS 2[30,31]. A population size of $P = 250$ with $N_{gen} = 150$ generations was used. Multiple independent runs were conducted to ensure convergence to the parsimonious model ($N_{runs} = 10$). Mutation, crossover, and direct reproduction probabilities were set at $p_{mut} = 0.84$, $p_{cross} = 0.14$, $p_{dir} = 0.02$, respectively. All final symbolic regression models were built using a total number of genes of $n_{genes} = 5$. Datasets were divided into training and testing subsets following a conventional $80-20\%$ ratio, respectively. MATLAB R2020 (MathWorks, Natick, MA, USA) was used.

Fabrication

Kirigami meta-atoms, 1D and 2D arrays were fabricated using an LPKF Protolaser R laser cutter (LPKF Laser & Electronics, Tualatin, USA) housed in Northwestern University's Micro/Nano Fabrication Facility. The substrate material was Kapton HN200 (Dupont, Wilmington, USA). Samples for Moire imaging were spray coated with white aerosol to allow for contrast.

Experiments

Tensile experiments were conducted using a micro-mechanical testing platform (Ernest F. Fullam Inc.) under displacement control at constant quasi-static rates. Force-displacements were recorded. Shadow Moire interferograms were obtained using a commercial chrome on glass Ronchi Ruling of 100 line pairs per inch (Edmund Optics, Barrington, USA). Shadow Moire configuration with light source and observation in the same plane was chosen ($L = 350$ mm). The observation was performed at a normal angle (camera to sample distance $L = 310$ mm) by means of a Mako U-503B CCD Monochrome Camera (Allied Vision Technologies GmbH) with 5 Megapixel resolution after passage through a 1x objective. Images were post-processed in Adobe Photoshop (Adobe, San Jose, CA, USA) for brightness and contrast adjustment only. One-dimensional post-processing (grating removal, signal filtering, and displacement calculations) was performed using an in-house developed code in MATLAB R2020. For more details of the experimental setup and post-processing, the reader is referred to our previous work on Kirigami using Shadow Moire[8].

DATA AVAILABILITY

The data that supports the findings of this study are available from the authors upon reasonable request.

CODE AVAILABILITY

The codes developed in this study are available from the authors upon reasonable request.

Received: 29 March 2022; Accepted: 8 August 2022;
Published online: 06 September 2022

REFERENCES

1. Yang, Y., Vella, K. & Holmes, D. P. Grasping with kirigami shells. *Sci. Robot.* **6**, eabd6426 (2021).
2. Rafsanjani, A. et al. Kirigami skins make a simple soft actuator crawl. *Sci. Robot.* **3**, eaar7555 (2018).
3. Song, Z. M. et al. Kirigami-based stretchable lithium-ion batteries. *Sci. Rep.* **5**, 10988 (2015).
4. Xu, K. C. et al. Highly stable kirigami-structured stretchable strain sensors for perdurable wearable electronics. *J. Mater. Chem. C.* **7**, 9609–9617 (2019).
5. Liu, Z. G. et al. Nano-kirigami with giant optical chirality. *Sci. Adv.* **4**, eaat4436 (2018).
6. Babaee, S. et al. Bioinspired kirigami metasurfaces as assistive shoe grips. *Nat. Biomed. Eng.* **4**, 778–786 (2020).

7. Zhang, X. et al. Kirigami engineering-nanoscale structures exhibiting a range of controllable 3D configurations. *Adv. Mater.* **33**, 2005275 (2021).
8. Alderete, N. A. et al. Programmable 3D structures via Kirigami engineering and controlled stretching. *Extrem. Mech. Lett.* **43**, 101146 (2021).
9. Jin, L. S. et al. Kirigami-inspired inflatables with programmable shapes. *Adv. Mater.* **32**, 2001863 (2020).
10. Hong, Y. Y. et al. Boundary curvature guided programmable shape-morphing kirigami sheets. *Nat. Commun.* **13**, 530 (2022).
11. Choi, G. P. T., Dudte, L. H. & Mahadevan, L. Programming shape using kirigami tessellations. *Nat. Mater.* **18**, 999–1004 (2019).
12. Bessa, M. A., Glowacki, P. & Houlder, M. Bayesian machine learning in metamaterial design: fragile becomes supercompressible. *Adv. Mater.* **31**, 1904845 (2019).
13. Kumar, S., Tan, S. H., Zheng, L. & Kochmann, D. M. Inverse-designed spinodoid metamaterials. *Npj Comput. Mater.* **6**, 73 (2020).
14. Hanakata, P. Z., Cubuk, E. D., Campbell, D. K. & Park, H. S. Accelerated search and design of stretchable graphene kirigami using machine learning. *Phys. Rev. Lett.* **121**, 255304 (2018).
15. Hanakata, P. Z., Cubuk, E. D., Campbell, D. K. & Park, H. S. Forward and inverse design of kirigami via supervised autoencoder. *Phys. Rev. Res* **2**, 042006 (2020).
16. Kim, B., Lee, S. & Kim, J. Inverse design of porous materials using artificial neural networks. *Sci. Adv.* **6**, eaax9324 (2020).
17. Liu, D. J., Tan, Y. X., Khoram, E. & Yu, Z. F. Training deep neural networks for the inverse design of nanophotonic structures. *Acs Photonics* **5**, 1365–1369 (2018).
18. Chen, C. T. & Gu, G. X. Generative deep neural networks for inverse materials design using backpropagation and active learning. *Adv. Sci.* **7**, 1902607 (2020).
19. Dias, M. A. et al. Kirigami actuators. *Soft Matter* **13**, 9087–9092 (2017).
20. Gao, L. et al. A bidirectional deep neural network for accurate silicon color design. *Adv. Mater.* **31**, 1905467 (2019).
21. Wiecha, P. R., Arbouet, A., Girard, C. & Muskens, O. L. Deep learning in nanophotonics: inverse design and beyond. *Photonics Res.* **9**, B182–B200 (2021).
22. Bessa, M. A. & Pellegrino, S. Design of ultra-thin shell structures in the stochastic post-buckling range using Bayesian machine learning and optimization. *Int. J. Solids Struct.* **139**, 174–188 (2018).
23. Santos, L. F., Silva, A. S., Correia, C. R. & Mano, J. F. Physical immobilization of particles inspired by pollination. *Proc. Natl Acad. Sci. USA* **116**, 5405–5410 (2019).
24. Ju, J. et al. A multi-structural and multi-functional integrated fog collection system in cactus. *Nat. Commun.* **3**, 1247 (2012).
25. Kim, Y. et al. Deep learning framework for material design space exploration using active transfer learning and data augmentation. *Npj Comput. Mater.* **7**, (2021).
26. Land, M. F. Animal eyes with mirror optics. *Sci. Am.* **239**, 126–134 (1978).
27. Hu, J., Bandyopadhyay, S., Liu, Y. H. & Shao, L. Y. A review on metasurface: from principle to smart metadevices. *Front. Phys.* **8**, 586087 (2021).
28. Zhang, Y. J. & Ye, W. J. Deep learning-based inverse method for layout design. *Struct. Multidiscip. Optim.* **60**, 527–536 (2019).
29. Paszke, A. et al. PyTorch: an imperative style, high-performance deep learning library. In *Advances in Neural Information Processing Systems 32* (eds Larochelle, H. et al.) 8024–8035 (2019).
30. Searson, D. P. in *Handbook of Genetic Programming Applications* (eds Gandomi, A. H., Alavi, A. H. & Ryan, C.) Ch. 22 (Springer International Publishing, 2015).
31. Searson, D. P., Leahy, D. E. & Willis, M. J. in *International Multiconference of Engineers and Computer Scientists* (IMECS, 2010).

ACKNOWLEDGEMENTS

H.D.E. acknowledges the financial support from a Multi-University Research Initiative through the Air Force Office of Scientific Research (AFOSR-FA9550-15-1-0009), NSF through award No. CMMI-1953806, and Army Research Office (ARO) through awards W911NF1510068. N.A.A. and H.D.E. gratefully acknowledge financial support from the Roberto Rocca Education Program (RREP). This work made use of the NUFAB facility of Northwestern University's NUANCE Center, which has received support from the SHyNE Resource (NSF ECCS-2025633), the IIN, and Northwestern's MRSEC program (NSF DMR-1720139).

AUTHOR CONTRIBUTIONS

N.A.A. and N.P. contributed equally to this work. N.A.A. and H.D.E. initiated the concept. N.A.A. performed and automated finite element simulations and other modeling tasks. N.A.A. fabricated Kirigami samples, performed experiments, and analyzed Moire images. N.P. performed clustering and neural network analyses. N.A.A. performed symbolic regression. Applications were conceived by all authors. All authors contributed to the data analysis and wrote the paper.

COMPETING INTERESTS

The authors declare no competing interests.

ADDITIONAL INFORMATION

Supplementary information The online version contains supplementary material available at https://doi.org/10.1038/s41524-022-00873-w.

Correspondence and requests for materials should be addressed to Horacio D. Espinosa.

Reprints and permission information is available at http://www.nature.com/reprints

Publisher's note Springer Nature remains neutral with regard to jurisdictional claims in published maps and institutional affiliations.